

# Optimizing the Time Between Reaction Wheel Desaturation Maneuvers

Malachi Mayfield\* and Àlvaro Romero-Calvo†

**Spacecraft equipped with reaction wheels require momentum management as part of nominal on-orbit operations. When chemical thrusters are used for dumping momentum, the maneuver may disturb sensitive payload operations. This paper presents an angular momentum management algorithm for planning the optimal desaturation strategy that maximizes the time between maneuvers. The algorithm is derived by applying solutions to the minimum enclosing disk problem to reaction wheel arrays. The algorithm provides a general technique for planning desaturation maneuvers, in contrast to current methods which are either too complex or too mission-specific. Simulation results show that its application can nearly double the time between maneuvers with respect to percentage based desaturation techniques.**

## I. Introduction

Many modern satellites depend on reaction wheel arrays (RWAs) for fine attitude control and momentum management. Typically, these RWAs consist of a minimum of 3 non-coplanar reaction wheels (RWs), allowing for 3-axis control. Often more than 3 RWs are used in an array, ensuring full attitude control can be maintained in the case of a wheel failure [1]. Although RWAs are versatile actuators, they have a finite amount of angular momentum storage capacity. As a consequence, momentum management is an important factor dictating spacecraft operations and lifespan.

When a RW becomes fully saturated, it loses the ability to produce a torque in the spin direction, potentially leading to attitude control issues for the spacecraft. To avoid this situation, a desaturation maneuver is performed before full saturation. These maneuvers, also called momentum unloads or momentum biasing, are accomplished by offloading angular momentum through the use of additional actuators such as magnetorquers, reaction control thrusters, or external environmental factors [2]. Near-Earth missions commonly rely on the magnetic field and the atmosphere to produce magnetic or atmospheric moments for continuous dumping and control of angular momentum [2, 3]. For spacecraft orbiting outside of the influence of Earth's magnetic field and atmosphere such as in GEO, Lunar, or interplanetary orbits, chemical thrusters or solar radiation torques are often the only option for momentum dumping [4]. When the spacecraft attitude is fully constrained, solar radiation torques act as a disturbance and thrusters must be used, usually in discrete maneuvers. Spacecraft operating in these orbits with payloads necessitating stringent pointing requirements often require normal payload operation to be suspended in order to accomplish these momentum unload maneuvers [5]. It is advantageous to extend the time between desaturation maneuvers for these missions, in turn increasing the useful time for payload operation.

Several different strategies exist for unloading momentum when RWAs are saturated. The most basic technique is to target a zero momentum value. While being the simplest, this does not maximize the time until the next desaturation. Instead, a biased momentum value may be targeted in order to increase the time until the next maneuver, given that the future state can be predicted. Due to the importance of extending the operational lifetime of spacecraft, methods of computing the optimal bias momentum target have been previously explored. It has been shown that predictive, rather than reactive momentum desaturation maneuvers can increase the time between maneuvers [6]. For on-orbit operations of the Tracking and Data Relay Satellite System (TDRSS) spacecraft, a system was constructed to present expert operators with future angular momentum predictions [7]. Operators used these predictions, along with intuition, to develop angular momentum unload plans for the spacecraft. For the GK-2A spacecraft, a technique was developed to bias the desaturation momentum for geostationary orbit [8]. However, the geometry of the problem and assumptions of constant disturbance torque and orthogonality between motion and accumulation limit the application for more complex situations. In cases such as the Cassini spacecraft, avoiding low wheel speeds was crucial for extending the lifespan of the RW bearings. As a consequence, the Reaction Wheel Bias Optimization Tool (RBOT), was developed [9]. Because of the focus on the prediction of individual wheel speeds, a significant level of complexity was introduced, likely unnecessary for most missions. During the development of the space station, a continuous control strategy for predictive

---

\*Graduate Student, Daniel Guggenheim School of Aerospace Engineering, Georgia Institute of Technology, lmayfield3@gatech.edu

†Assistant Professor, Daniel Guggenheim School of Aerospace Engineering, Georgia Institute of Technology, romerocalvo@gatech.edu

momentum management using control moment gyros was outlined [2]. This controller makes use of the reaction control system when additional control torque is required, focusing the method on continuous angular momentum control rather than discrete unload maneuvers. While these works provide a variety of momentum management techniques, the applications and assumptions are largely limited to specific missions. A broader technique for optimally planned momentum management maneuvers, applicable to many missions is needed.

To accomplish these goals, this paper presents and evaluates an optimal desaturation planning algorithm. The algorithm applies a linear programming result for determining minimum bounding spheres to the problem of momentum management. Utilizing the desired future attitude profile and predicted external disturbances, an optimal momentum target profile is generated for the RWA.

The remainder of this paper is organized as follows. In the following section, the system and assumptions are introduced, the dynamical system describing the time evolution of the RWA is derived, and the general optimization problem is presented. In Section III, the optimal algorithm is detailed. Section IV compares the optimal algorithm to other techniques through simulation of the proposed Lunar Meteoroid Impact Observer (LUMIO) mission profile [10]. Lastly, Section V describes the future work applicable to the optimal planning algorithm.

## II. Problem Formulation

To make predictions about the future state of a spacecraft, the scope of the problem must be limited to cases with given future attitude profiles. An understanding of the future attitude state is critical for predicting the exchange of momentum between the spacecraft body and the RWA. For missions with predefined orbits and pointing targets, the future attitude profile is well-defined. In addition, an accurate disturbance torque model is crucial for predicting the evolution of the total angular momentum of the system. One key assumption of the following derivation is that the spacecraft follows the desired attitude profile exactly, excluding the impact of a controller.

When describing the state of the RWA, different state variables lend themselves to different cases. For control purposes, individual wheel parameters are often of use. Examples include individual wheel speed, spin axis, or momentum. These each may be expressed in a RW, body-fixed, or inertial frames. For the purposes of momentum management, it is advantageous to represent the state as the sum of the angular momentum of each wheel, either expressed in a body-fixed or inertial frame. This state is not necessarily unique, however when expressed in this way, desaturation occurs when this vector exceeds the momentum envelope of the RWA.

### A. RWA Dynamical System

To identify an optimal angular target for a desaturation maneuver, an expression describing the evolution of the angular momentum of the RWA is essential. To develop this, we begin with an expression for the net angular momentum of a spacecraft in the inertial frame,  $\mathbf{h} = \mathbf{h}_b + \mathbf{h}_w$ , where the time dependency is omitted for clarity.  $\mathbf{h}_b = \mathbf{J}\boldsymbol{\omega}$  represents the spacecraft body angular momentum and  $\mathbf{h}_w$  represents the total angular momentum stored by the RWA.

Euler's second law specifies that in an inertial frame, the time rate of change of angular momentum is equal to the external moments. Applying this to the expression for  $\mathbf{h}$  yields [1]

$$\frac{d\mathbf{h}_b^N}{dt} + \frac{d\mathbf{h}_w^N}{dt} = \mathbf{M}, \quad (1)$$

with the superscript denoting the frame in which the derivative is taken. Using the vector transport theorem, the time rate of change of the spacecraft body term can be expressed in the rotating body fixed frame as

$$\mathbf{J} \frac{d\boldsymbol{\omega}^B}{dt} + \boldsymbol{\omega} \times \mathbf{J}\boldsymbol{\omega} + \frac{d\mathbf{h}_w^N}{dt} = \mathbf{M}, \quad (2)$$

where  $\boldsymbol{\omega}$  is the angular velocity of the body frame with respect to the inertial frame and  $\mathbf{J}$  is the spacecraft inertia matrix in the body frame, assumed to be constant. Rearranging Eq. 2 to solve for the inertial time rate of change of the RWA angular momentum results in

$$\frac{d\mathbf{h}_w^N}{dt} = \mathbf{M} - \mathbf{J} \frac{d\boldsymbol{\omega}^B}{dt} - \boldsymbol{\omega} \times \mathbf{J}\boldsymbol{\omega}. \quad (3)$$

Equation 3 describes the time evolution of the angular momentum of the RWA in response to the specified attitude profile and known external disturbances.

## B. Optimization Problem

With the dynamics of the RWA defined, the desaturation planning and targeting task can be represented as a constrained optimization problem. The problem is taken at a given starting time,  $t_0$ , with the goal of maximizing the final time,  $t_f$ , at which point saturation first occurs.

Saturation occurs when the total RWA angular momentum,  $\mathbf{h}_w$ , reaches the boundary of the angular momentum envelope of the RWA. In general, the total angular momentum envelope of a RWA is determined by a  $n$ -dimensional hypercube projected into  $\mathbb{R}^3$  where  $n$  is the number of RWs [11]. This angular momentum envelope is defined by the spin axes and maximum momentum storage capabilities of each RW in the array. Because this general case is dependent on the exact orientation and storage capacity of each RW, the saturation condition is dependent on the attitude of the spacecraft in addition to  $\mathbf{h}_w$ . To simplify this complexity, for the defining saturation, the angular momentum envelope is assumed to be the sphere of radius  $h_{max}$  that is inscribed in the true momentum envelope. By making this assumption, the saturation condition is no longer attitude dependent albeit at the cost of underestimating true storage capacity. For RWAs consisting of approximately uniformly oriented RWs with similar storage capacity, this underestimation is likely insignificant.

Compiling the constraints on the RWA dynamics, performance object, and saturation condition yields the optimization problem

$$\max_{\mathbf{h}_0} t_f \quad (4a)$$

s.t.

$$\frac{d\mathbf{h}_w^N}{dt} = \mathbf{M} - \mathbf{J} \frac{d\boldsymbol{\omega}^B}{dt} - \boldsymbol{\omega} \times \mathbf{J} \boldsymbol{\omega} \quad (4b)$$

$$\|\mathbf{h}_w(t)\| < h_{max}, \quad t_0 \leq t < t_f \quad (4c)$$

$$\|\mathbf{h}_w(t_f)\| = h_{max} \quad (4d)$$

$$\mathbf{h}_w(t_0) = \mathbf{h}_0 \quad (4e)$$

$$(4f)$$

Because the attitude profile,  $\boldsymbol{\omega}$  and its time rate of change, and external disturbance torques,  $\mathbf{M}$ , are all predefined, the only influence on the problem is through the initial condition  $\mathbf{h}_0$ . This initial condition is the desaturation target, as desaturating the RWA to this angular momentum maximizes the time until the next saturation condition occurs.

## III. Methods

Considering that in the general case, the attitude profile and external disturbances are entirely arbitrary, there does not exist a closed-form solution for  $\mathbf{h}_0$ . Despite this, by using the geometry of the problem, the solution can be found using an iterative binary search.

### A. Geometrical Interpretation

Although not explicitly expressed, the RWA dynamics are solely dependent on time through the time dependent profiles of  $\mathbf{M}$  and  $\boldsymbol{\omega}$ . Reintroducing the time dependency, Eq. 3 can be rewritten as

$$\frac{d\mathbf{h}_w^N}{dt}(t) = \mathbf{M}(t) - \mathbf{J} \frac{d\boldsymbol{\omega}^B}{dt}(t) - \boldsymbol{\omega}(t) \times \mathbf{J} \boldsymbol{\omega}(t). \quad (5)$$

Due to the dependence on time alone, this differential equation has the trivial solution of the form

$$\mathbf{h}_w(t) = \mathbf{h}_w(t_0) + \mathbf{c}(t) \quad t \in [t_0, t_f], \quad (6)$$

with  $\mathbf{c}(t)$  describing the trajectory taken by  $\mathbf{h}_w$  in the inertial frame, defined as

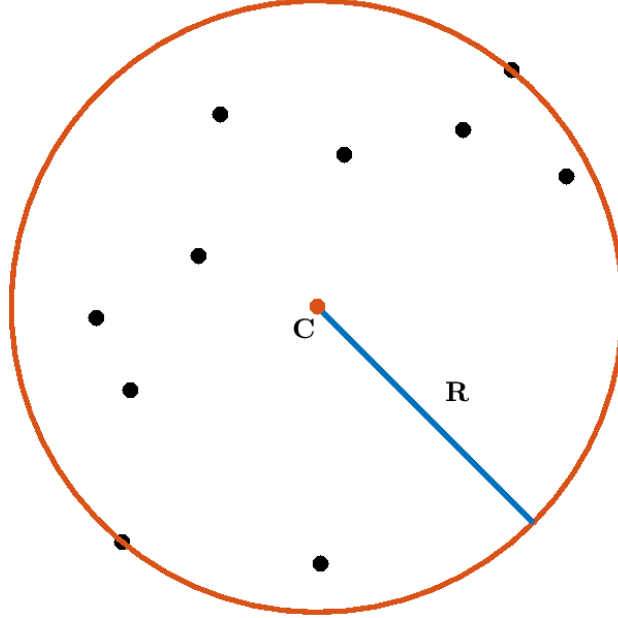
$$\mathbf{c}(t) = \int_{t_0}^{t_f} \left[ \mathbf{M}(t) - \mathbf{J} \frac{d\boldsymbol{\omega}^B}{dt}(t) - \boldsymbol{\omega}(t) \times \mathbf{J} \boldsymbol{\omega}(t) \right] dt. \quad (7)$$

Because of the single dependence on time,  $\mathbf{c}(t)$  is entirely predetermined, which constrains  $\mathbf{h}_w(t)$ , with the exception that it can be translated by  $\mathbf{h}_0$ . The saturation constraints of Eq. 4 also have a simple geometrical interpretation. The 3D

path taken by  $\mathbf{h}_w(t)$  must remain inside the defined momentum envelope, the sphere of radius  $h_{max}$ , until  $t_f$ , at which point it intersects the boundary.

The smallest sphere that perfectly encloses a set of points is defined as the minimum enclosing sphere. Every set of points has a minimum enclosing sphere, which in general is not centered at the origin. Figure 1 shows a 2D minimum enclosing disk with center,  $C$ , and radius,  $R$  for a set of points.

**Fig. 1 Minimum Enclosing Disk**



To exploit the geometry of the problem, it is important to note that for the optimal solution, the minimum enclosing sphere of  $\mathbf{h}_w(t), t \in [t_0, t_f]$  is equivalent to the momentum envelope, a sphere of radius  $h_{max}$  centered at the origin. If the minimum enclosing sphere of  $\mathbf{h}_w(t)$  were to have a radius greater than  $h_{max}$ , the desaturation condition would occur prior to  $t_f$  and the solution would not be optimal. Conversely, if the minimum enclosing sphere of  $\mathbf{h}_w(t)$  were to have a radius less than  $h_{max}$ , the desaturation condition will occur after  $t_f$ , signifying that the solution is also not optimal. Therefore, finding the optimal solution is equivalent to finding the minimum enclosing sphere of radius  $h_{max}$ , centered at the origin.

Despite this fact, both  $\mathbf{h}_w(t)$  and  $t_f$  are unknown, making the problem difficult to solve. However, it has been established that  $\mathbf{h}_w(t)$  is equivalent to  $\mathbf{c}(t)$  through the translation of  $\mathbf{h}_0$ . As a result, when finding the minimum enclosing sphere, the location of the center is irrelevant since it can always be translated to the origin with  $\mathbf{h}_0$ . This indicates that finding the minimum enclosing sphere of  $\mathbf{h}_w(t)$  with a radius  $h_{max}$  is identical to finding the minimum enclosing sphere of  $\mathbf{c}(t)$  with a radius  $h_{max}$ . This fact allows the solution to be found simply because  $\mathbf{c}(t)$  is known, while  $\mathbf{h}_w(t)$  is not. This reduces the problem to one variable to search,  $t_f$ . By finding the time,  $t_f$  in which the minimum enclosing sphere of  $\mathbf{c}(t), t \in [t_0, t_f]$  has a radius equivalent to  $h_{max}$  the problem has been solved. To recover the desired initial condition  $\mathbf{h}_0$ , the sphere is translated to zero, resulting in

$$\mathbf{h}_0 = -\mathbf{C} . \quad (8)$$

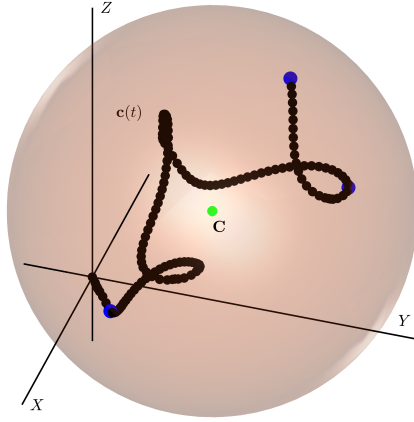
Thus, the desaturation target can be found through the parameters of the minimum enclosing sphere of  $\mathbf{c}(t)$  alone. In Fig. 2a, 2b the relationships between  $\mathbf{h}_0, \mathbf{c}(t)$ , and  $\mathbf{h}_w(t)$  are shown. In the interior of the minimum enclosing sphere, defined by blue points on the surface, the trajectories of  $\mathbf{c}(t)$ , and  $\mathbf{h}_w(t)$  appear identical, except for the translation that brings  $C$  to the center. In this example, the point  $\mathbf{h}_0$  does not lie on the surface, although it is generally possible.

## B. Welzl's Algorithm

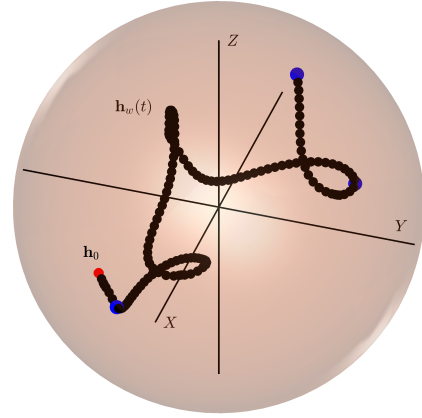
In order to determine the sphere that minimally encloses a set of points, Welzl's algorithm is used [12]. This algorithm finds the solution to the minimum enclosing sphere problem in linear time. To accomplish this, the algorithm

**Fig. 2 Minimum Sphere Translation**

**(a) Minimum enclosing sphere of  $c(t)$**



**(b) Minimum enclosing sphere of  $h_w(t)$**



recursively iterates over each point in the set, determining if it is enclosed by the sphere or should belong to the boundary.

To begin the search, a random point is removed from the set. For the first point, the minimum enclosing sphere is centered at the point with radius 0. Because of this, the single point is saved to a set of points defining the minimum enclosing sphere. This continues for the second point which is removed from the set of overall points but added to the set of surface points because an analytic solution is available. The minimum enclosing sphere has a center halfway between the points and a radius equal to half the distance between them. The next random point may lie inside the sphere defined previously or it may lie on the exterior. For the case that lies inside, the point is neglected and iteration continues on the remaining points. If the point is located outside of the previous sphere, it must be part of the new enclosing sphere. The new sphere is calculated by trying combinations of points in the set of 2 or 3 sphere points. Once the new minimum enclosing sphere is determined, any sphere points that are now on the interior are removed. This iteration continues, removing a random point and determining if it is inside the sphere until no points remain. When this happens, the unique minimum enclosing sphere is found.

### C. Binary Search Algorithm

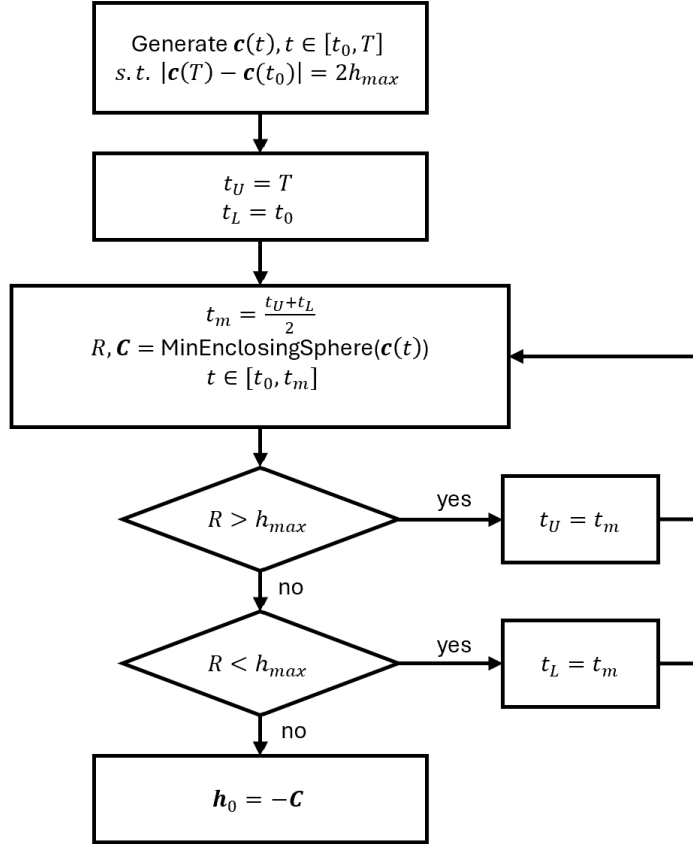
In order to apply Welzl's algorithm to this problem,  $c(t)$  must be discretized into  $n$  points. This takes place naturally when computed using numerical integration. Upon doing this, the algorithm locates the center,  $C$ , and radius,  $R$ , of the minimum enclosing sphere in linear time.

Because the algorithm searches along  $c(t)$ , that profile is first calculated sufficiently far into the future such that a saturation condition occurs in the time interval. This can be accomplished by computing until  $T$ , the first time at which  $\|c(T)\| = 2h_{max}$ . Over the time interval  $[t_0, T]$ , the minimum enclosing sphere has at least a radius  $h_{max}$ , guaranteeing the solution can be found.

With a sufficient time interval, the algorithm is initialized with a lower bound of  $t_L = t_0$  and an upper bound of  $t_U = T$ . Next, the midpoint of the interval,  $t_m$  is calculated and the minimum bounding sphere is calculated using the interval between the lower bound and the midpoint. If the radius of the sphere,  $R$  is greater than  $h_{max}$ , this means that the optimal  $t_f$  exists in the lower half of the interval and the next upper bound is set to  $t_m$ . In the case where  $R < h_{max}$ , the optimal  $t_f$  exists in the upper half of the interval and the next lower bound is set to  $t_m$ . This process repeats until  $R$  converges to  $h_{max}$ . Once this condition occurs, the center is used in Eq. 8 to find  $h_0$ . In Fig. 3, the flow chart describes the execution of the algorithm for a single point in time. For subsequent searches, the search interval becomes much shorter because the lower bound is set to the  $t_f$  of the previous solutions.

After finding the solution at  $t_0$ , this process of finding  $h_0$  may be repeated for additional times into the future, effectively generating a profile of desaturation targets. The exact process presented above may be used for a time  $t_0 + \Delta t$ . However, by using the previous solution, the search interval can be reduced. To do this,  $c(t)$  may need to be computed further such that  $\|c(t_U) - c(t_0 + \Delta t)\| = 2h_{max}$ . With additional points, it is already known that all points between

**Fig. 3 Binary Search Algorithm**



$t_0 + \Delta t$  and the previous  $t_f$  solution exist in the sphere. As a consequence,  $t_L = t_f$  and the search interval is significantly reduced. The binary search is then run on this smaller interval. Once the optimal initial condition is computed for all desired future times, an optimal desaturation target profile is achieved. This target profile is represented in the inertial frame, and when a specific momentum target is needed, it must be transformed into the current body frame for use in most desaturation control schemes.

#### D. Simulation Setup

The LUMIO CubeSat mission is used as a baseline to compare the optimal desaturation technique [10]. The primary aim of the LUMIO mission is to observe meteoroid impacts on the far side of the moon. To accomplish this, the CubeSat will occupy a halo orbit around the Earth-Moon L2 point, providing continuous observation of the lunar far side. The spacecraft has an attitude fixed by the directions of the moon and sun to provide both observation and power generation. In the halo orbit, solar radiation torque is the most significant attitude disturbance.

The dynamics of the spacecraft equipped with RWs are governed by the equations of motion [1]

$$J\dot{\omega} + \omega \times J\omega = \mathbf{u}_w + \mathbf{d}, \quad (9)$$

$$\dot{\mathbf{h}}_w = -R^*(\mathbf{u}_c + \omega \times R\mathbf{h}_w), \quad (10)$$

$$\mathbf{u}_w = -A\dot{\mathbf{h}}_w - \omega \times R\mathbf{h}_w^s, \quad (11)$$

where the control moment is  $\mathbf{u}_w$ , the external disturbance moment is  $\mathbf{d}$ ,  $A$  is the inertial to body Direction Cosine Matrix (DCM), and  $R$  is the actuator matrix describing RW spin axes. The superscript "s" terms describe the respective variables after saturation. The "\*" operator is defined as the pseudo-inverse.

The desired attitude profile is defined such that the imaging payload, oriented in the  $+x$  direction always faces the moon. The  $+y$  direction is then constrained to a direction orthogonal to both the sun and the moon. This allows the solar arrays, oriented in the  $+z$  direction to always minimize the angle to the sun. This results in the desired attitude DCM

$$A_d = \begin{bmatrix} \mathbf{x}_1 = \mathbf{x}^M \\ \mathbf{x}_2 = \frac{\mathbf{x}^S \times \mathbf{x}^M}{\|\mathbf{x}^S \times \mathbf{x}^M\|} \\ \mathbf{x}_3 = \frac{\mathbf{x}^M \times \mathbf{x}_2}{\|\mathbf{x}^M \times \mathbf{x}_2\|} \end{bmatrix}, \quad (12)$$

where  $\mathbf{x}^M$  and  $\mathbf{x}^S$  represent the directions to the moon and sun, respectively.

The attitude control law allocated to the RWA is given by

$$\mathbf{u}_w = -k_1 \boldsymbol{\omega}_e - k_2 (A_e^T - A_e)^V + \boldsymbol{\omega} \times J \boldsymbol{\omega} + J (A_e \dot{\boldsymbol{\omega}}_d - [\boldsymbol{\omega}_e]_e^A \boldsymbol{\omega}_d) - \mathbf{d} - \mathbf{u}_d, \quad (13)$$

where  $\boldsymbol{\omega}_e$  and  $A_e$  are the angular velocity and attitude DCM error.  $\boldsymbol{\omega}_d$  is the desired angular velocity.  $k_1$  and  $k_2$  are control gains. The  $V$  superscript denotes the hat map and the  $\wedge$  superscript represents the inverse hat map. The desaturation control torque, allocated to the thrusters, is given as

$$\mathbf{u}_d = k_3 R (\mathbf{h}_w - \mathbf{h}_w^d) - \boldsymbol{\omega} \times R \mathbf{h}_w, \quad (14)$$

where  $\mathbf{h}_w^d$  is the desired RWA momentum and  $k_3$  is another control gain.  $\mathbf{u}_d$  is set to zero whenever desaturation maneuvers are not taking place. The only disturbance included in the simulation is solar radiation torque. The spacecraft is assumed to be made of 10 surfaces such that the solar radiation disturbance torque is given by

$$\mathbf{d} = \sum_{i=1}^n \mathbf{c}_{pi} \times \mathbf{F}_i, \quad (15)$$

where  $\mathbf{c}_{pi}$  and  $\mathbf{F}_i$  represent the center of pressure and the solar radiation force of the  $i$ -th surface. Each force,  $\mathbf{F}_i$ , is equal to zero if the surface normal is not oriented facing the sun's direction.

These governing equations were solved in a year-long Simulink simulation of the LUMIO attitude control system in order to evaluate the desaturation techniques. The attitude dynamics, controller, disturbances, and desaturation logic are all included in the simulation and held constant across the different desaturation techniques. The control gains used were  $k_1 = 0.0005$ ,  $k_2 = 0.0005$ , and  $k_3 = 0.01$ . Each RW has a maximum angular momentum storage of 0.03 Nms. In the RWA, 3 RWs are oriented with spin directions along the body axes. The desaturation condition is set to a value of 0.027 Nms to avoid full saturation of wheels.

To allow for margin in the momentum management system, to compute the optimal angular momentum target profile, a value of  $h_{max} = 0.025$  Nms is used, 90% of the true maximum angular momentum storage capability of the RW. The desired attitude profile is used to compute the predicted disturbance torque. These are used together to compute the optimal desaturation target profile, following the methods described in Section III. The profile is generated for a year-long time frame. In Fig. 4, the optimal desaturation target profile is shown for a 150-day subset of the year in the inertial frame. The periodicity of the lunar cycle is seen in the optimal profile as the general pattern repeats every 30 days.

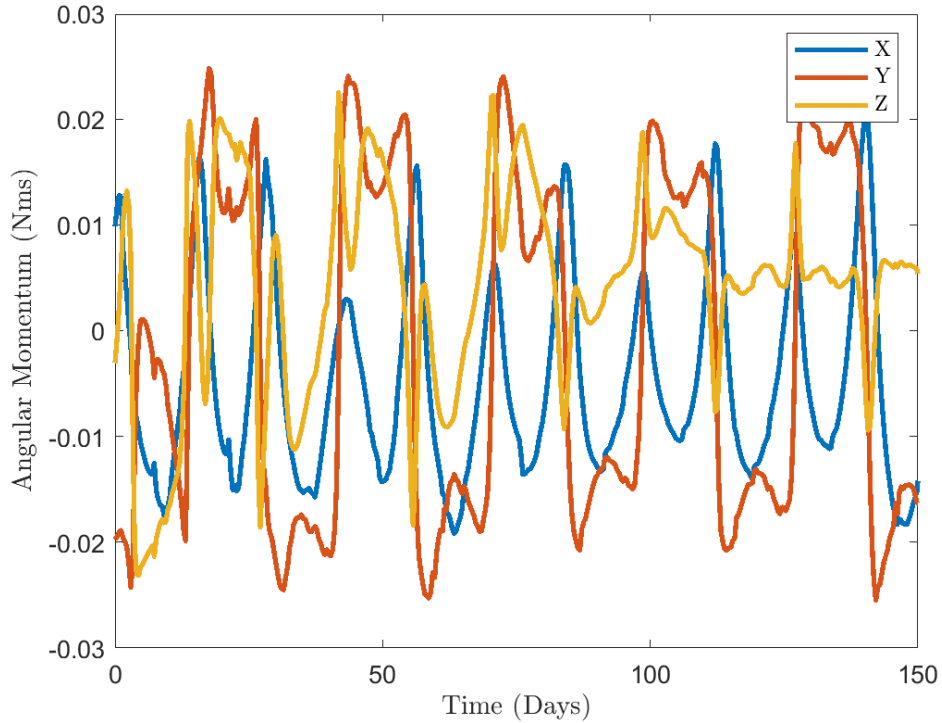
To evaluate the optimal desaturation technique, 4 other desaturation strategies are also simulated. In these simulations, when the desaturation condition is reached, each axis unloads momentum until the angular momentum reaches a specified percentage of  $h_{max}$ : 70%, 50%, 30%, and 0%. This strategy strictly decreases the magnitude of  $\mathbf{h}_w$ . In the final simulation, the optimal technique introduced in this paper is used. For the optimal case and 0% maneuver, the desaturation maneuver is considered complete when the magnitude of the difference between  $\mathbf{h}$  and the target was less than 0.001 Nms. For the percentage-based desaturation strategies, the maneuver is complete when the angular momentum of all axes falls below the specified percentage of maximum. Each simulation was run for 365 days, in order to gain insight into the long-term patterns of each technique.

## IV. Results and Discussion

### A. Simulation Results

Over the 5 year-long simulations, the optimal approach resulted in a total of 5 desaturation maneuvers, while the 0%, 30%, 50%, and 70% targets resulted in 8, 11, 16, and 30 desaturation maneuvers, respectively. Figure 5 shows the

**Fig. 4 Desaturation Target Profile**



median time between desaturation maneuvers for each technique. As expected, the optimal approach maximizes this time. The optimal median duration of 56.02 days nearly doubles the next best approach, desaturating to 0%. This result is intuitive as the percentage-based approach can only use half of the momentum envelope while the optimal result can explore the entire space.

While the optimal technique does provide the longest time between maneuvers, it also comes at the cost of propellant usage. The optimal scheme resulted in a total impulse of 7.22 Ns used across all thrusters. In comparison the 0%, 30%, 50%, and 70% schemes used 7.53, 6.56, 5.58, 5.69 Ns each. For all of the simulations, the first 150 days experienced significantly fewer desaturation maneuvers. This is due to slower angular momentum accumulation during this time period in comparison to the remainder of the simulation time. Figure 6 shows how the impulse usage evolves over time for each of the desaturation schemes. The 0% scheme uses the most but is very comparable with the optimal technique. The reason for the increase in propellant usage is likely due to the increased thruster firing times because of the larger dumping of angular momentum required. Additionally, the increase in propellant usage may be attributed to the increased control effort required to precisely target a single point versus simply decreasing magnitude.

## V. Conclusions

The optimal angular momentum planning technique described in this paper is shown to optimize the time between desaturation maneuvers for a simple spacecraft. Welzl's algorithm for determining minimum enclosing spheres is applied to the predicted angular momentum profile to generate an optimal desaturation target profile. This profile ensures that every desaturation maneuver has an optimal target, optimizing the time until the next maneuver. The result is validated through simulations of the LUMIO spacecraft over a single year. The simplicity of the algorithm means that it can easily be applied to a variety of different spacecraft missions equipped with RWAs, as long as there is an ability to predict future disturbances and the attitude profile.

**Fig. 5 Median duration between desaturation maneuvers**

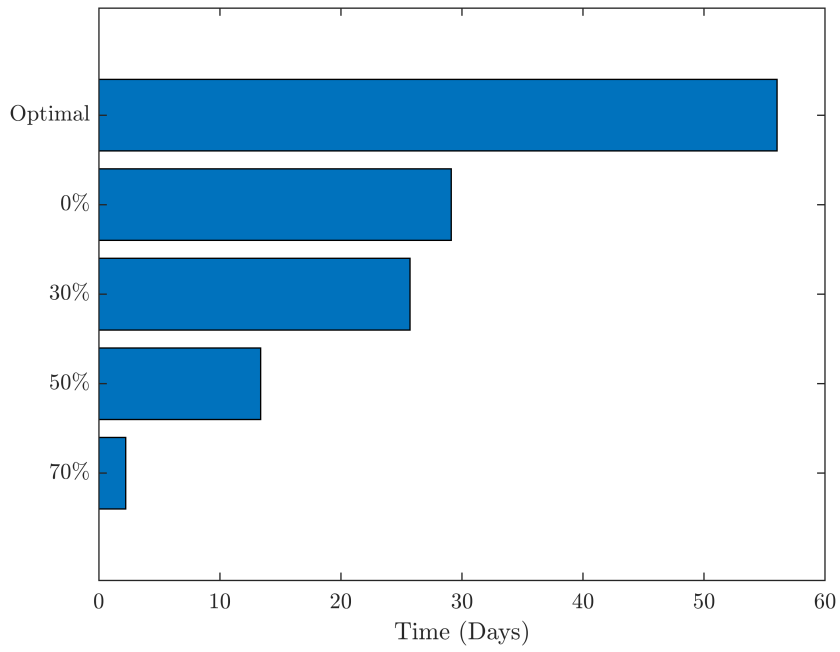
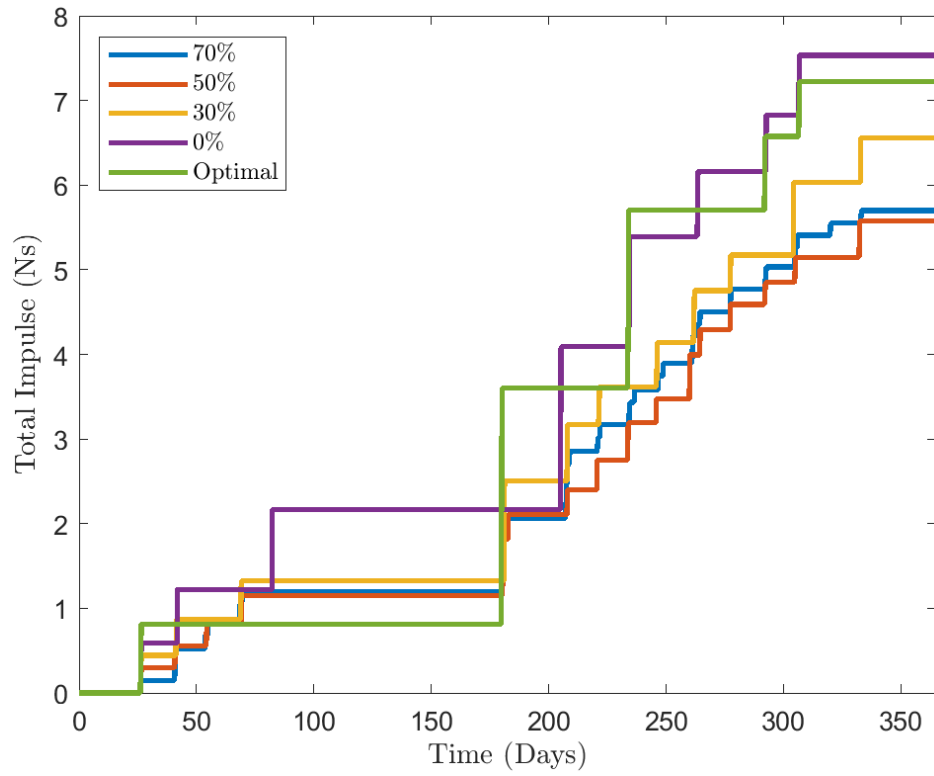


**Fig. 6 Total impulse used**



## References

- [1] Schaub, H., and Junkins, J. L., *Analytical Mechanics of Space Systems*, 4<sup>th</sup> ed., American Institute of Aeronautics and Astronautics, Inc., 2018.
- [2] Hattis, P. D., “Predictive momentum management for the Space Station,” *Journal of Guidance, Control, and Dynamics*, Vol. 9, No. 4, 1986, pp. 454–461. <https://doi.org/10.2514/3.20132>.
- [3] Camillo, P. J., and Markley, F., “Orbit-averaged behavior of magnetic control laws for momentum unloading,” *Journal of Guidance and Control*, Vol. 3, No. 6, 1980, pp. 563–568. <https://doi.org/10.2514/3.19725>.
- [4] Satpute, S., and Emami, M. R., “Concurrent station keeping and momentum management of geostationary satellites,” *The Journal of the Astronautical Sciences*, Vol. 66, No. 3, 2019, pp. 341–360. <https://doi.org/10.1007/s40295-019-00159-2>.
- [5] Kinzel, W. M., and Isaacs, J., “Momentum Management Operations Concept,” *Space Telescope Science Inst. TR JWST-STScI-001275, SM-12*, 2007. URL <https://citeseerx.ist.psu.edu/document?repid=rep1&type=pdf&doi=f8155481573ef671685bc6b84ab4bf9644c27e03>.
- [6] Vaughan, R. M., Haley, D. R., O’Shaughnessy, D. J., and Shapiro, H. S., “Momentum management for the MESSENGER mission,” *Advances in the Astronautical Sciences*, Vol. 109, 2002, pp. 1139–1158. URL <https://messenger.jhuapl.edu/Resources/Publications/Vaughan.et.al.2001.pdf>.
- [7] Cross, G. R., Potter, M. A., Whitehead, J. D., and Smith, J. T., “Knowledge-based TDRSS momentum unload planning,” *Telematics and Informatics*, Vol. 8, No. 4, 1991, pp. 253–265. [https://doi.org/10.1016/S0736-5853\(05\)80052-8](https://doi.org/10.1016/S0736-5853(05)80052-8), space Applications of Artificial Intelligence.
- [8] Yoon, H., Kim, H., Yun, J., and Yoon, H., “Momentum Management of Reaction Wheels for an Asymmetric Geostationary Satellite: with GK-2A Flight Data Analysis,” *AIAA SCITECH 2024 Forum*, 2024. <https://doi.org/10.2514/6.2024-1449>.
- [9] Lee, C., and Lee, A., “Cassini Reaction Wheel Momentum Bias Optimization Tool,” *AIAA Guidance, Navigation, and Control Conference and Exhibit*, 2012. <https://doi.org/10.2514/6.2005-6271>.
- [10] Romero-Calvo, A., Biggs, J., and Topputo, F., “Attitude Control for the LUMIO CubeSat in Deep Space,” *70th International Astronautical Congress (IAC 2019)*, 2019, pp. 1–13.
- [11] Markley, F., Reynolds, R., Liu, F., and Lebsack, K., “Maximum Torque and Momentum Envelopes for Reaction Wheel Arrays,” *AIAA Guidance, Navigation, and Control Conference*, 2001. <https://doi.org/10.2514/6.2009-6109>.
- [12] Welzl, E., “Smallest enclosing disks (balls and ellipsoids),” *New Results and New Trends in Computer Science*, edited by H. Maurer, Springer Berlin Heidelberg, Berlin, Heidelberg, 1991, pp. 359–370. <https://doi.org/10.1007/BFb0038202>.